A TROP2/Claudin Program Mediates Immune Exclusion to Impede Checkpoint Blockade in Breast Cancer

Bogang Wu[1], *Win Thant*[1], *Elena Bitman*[1], *Ting Liu*[1], *Jie Liu*[2], *Eleftherios I. Paschalis*[2], *Katherine H. Xu*[1], *Linda T. Nieman*[1], *David T. Ting*[1], *Nayana Thimmiah*[1], *Sheng Sun*[1], *Rachel O. Abelman*[1], *Steven J. Isakoff*[1], *Laura M. Spring*[1], *Aditya Bardia*[1], *Leif W. Ellisen*[1,3]

1- Massachusetts General Hospital Cancer Center, Harvard Medical School, Boston, MA 02114, USA

2- Massachusetts Eye and Ear, Harvard Medical School, Boston, MA, 02114, USA

3- Ludwig Center at Harvard, Boston, MA 02115, USA

Correspondence:

Dr. Leif W. Ellisen
MGH Cancer Center, 185 Cambridge St., CPZN-4204
Boston, MA 02114
(617) 726-4315
lellisen@mgh.harvard.edu

Key words: TROP2, Antibody-Drug Conjugate, sacituzumab govitecan, tight junction, triple negative breast cancer, PD-1, antitumor immunity, tumor immune microenvironment, immune checkpoint blockade, immune exclusion.

Running title:

TROP2 mediates immune exclusion to impede checkpoint blockade.

Conflict of Interest: D.T.T. has received consulting fees from ROME Therapeutics, Sonata Therapeutics, Tekla Capital, and abrdn. D.T.T. is a founder and has equity in ROME Therapeutics, PanTher Therapeutics and TellBio, Inc., which is not related to this work. D.T.T. is on the advisory board for ImproveBio, Inc. D.T.T. has received honorariums from AstraZeneca, Moderna, and Ikena Oncology that are not related to this work. D.T.T. receives research support from ACD-Biotechne, AVA LifeScience GmbH, Incyte Pharmaceuticals, and Sanofi, which was not used in this work. D.T.T.'s interests were reviewed and are managed by Massachusetts General Hospital and Mass General Brigham in accordance with their conflict of interest policies. S.J.I.: Institutional support from Genentech and Astra Zeneca. L.M.S.: Consultant/advisory board: Novartis, Daiichi Pharma, Astra Zeneca, Eli Lilly, Precede, Seagen; Institutional research support: Merck, Genentech, Gilead, Eli Lilly. A.B.: Consultant/advisory board: Pfizer, Novartis, Genentech, Merck, Radius Health; Immunomedics/Gilead, Sanofi, Daiichi Pharma/Astra Zeneca, Phillips, Eli Lilly, Foundation Medicine; Contracted Research/Grant (to institution): Genentech, Novartis, Pfizer, Merck, Sanofi, Radius Health, Immunomedics/Gilead, Daiichi Pharma/Astra Zeneca, Eli Lilly. L.W.E.: Consultant to Mersana,

Inc.; Consultant to Kisoji Biotech; Consultant to Astra Zeneca; Consultant to Gilead; Sponsored Research Agreement with Sanofi. The other authors declare no competing interests.

ABSTRACT

Immune exclusion inhibits anti-tumor immunity and response to immunotherapy, but its mechanisms remain poorly defined. Here, we demonstrate that Trophoblast Cell-Surface Antigen 2 (TROP2), a key target of emerging anti-cancer Antibody Drug Conjugates (ADCs), controls barrier-mediated immune exclusion in Triple-Negative Breast Cancer (TNBC) through Claudin 7 association and tight junction regulation. TROP2 expression is inversely correlated with T cell infiltration and strongly associated with outcomes in TNBC. Loss-of-function and reconstitution experiments demonstrate TROP2 is sufficient to drive tumor progression in vivo in a CD8 T cell-dependent manner, while its loss deregulates expression and localization of multiple tight junction proteins, enabling T cell infiltration. Employing a humanized TROP2 syngeneic TNBC model, we show that TROP2 targeting via hRS7, the antibody component of Sacituzumab govitecan (SG), enhances the anti-PD1 response associated with improved T cell accessibility and effector function. Correspondingly, TROP2 expression is highly associated with lack of response to anti-PD1 therapy in human breast cancer. Thus, TROP2 controls an immune exclusion program that can be targeted to enhance immunotherapy response.

Synopsis

This study defines a new mechanism of barrier-mediated immune exclusion in cancer controlled by TROP2-dependent tight junctions. This mechanism drives tumor progression but can be targeted via TROP2-directed antibody drug conjugates to activate anti-tumor immunity and enhance immunotherapy response.

INTRODUCTION

Within normal tissues, mechanical barriers are a major self-defense mechanism that serves to exclude invading pathogens, maintain tissue integrity, and precisely regulate permeability to unwanted immune infiltration that can damage healthy tissues [1, 2]. These barrier mechanisms are co-opted in diverse cancers, where emerging data suggest that extracellular matrix and intercellular junctions exclude immune cells and bioactive molecules as a mechanism of immune evasion [3-5]. Such barrier mechanisms are also recognized as an impediment that prevents many patients from deriving benefit from immunotherapy [6-9]. While barrier-mediated immune exclusion has been studied extensively in normal immune-privileged organs [10-12], a detailed understanding of its role in anti-tumor immunity is lacking.

Trophoblast cell surface antigen 2 (TROP2) is a transmembrane glycoprotein expressed on the cell surface in select epithelial tissues. TROP2 is also overexpressed in a variety of carcinomas, including triple negative breast cancer (TNBC), a highly aggressive subtype that contributes disproportionately to breast cancer morbidity and mortality [13, 14]. The potential contribution of TROP2 in cancer remains controversial, however. TROP2 overexpression has been implicated in a variety of tumor phenotypes including proliferation, survival, invasion and stem cell character, while other work suggests a contribution of TROP2 loss to tumorigenic cell signaling [15, 16]. Encoded by *TACSTD2*, TROP2 is a paralog of EpCAM and is comprised of extracellular, transmembrane and intracellular domains. Diverse signaling pathways that promote cancer phenotypes are reported to be activated by TROP2, including PI3K/AKT [17], MAPK/ERK [18], JAK/STAT [19], and β-catenin [20], in multiple cases attributed to signaling via the 26-amino acid intracellular domain. In contrast, Loss of TROP2 function is observed in human gelatinous drop-

like corneal dystrophy (GDLD), an inherited disease characterized by increased corneal basement membrane permeability [21-26]. Thus, substantial uncertainty exists regarding the critical functions and mechanisms of TROP2 in cancer.

TROP2 is now a major focus for cancer therapy, as it is the target of multiple recently-developed antibody-drug conjugates (ADCs), including Sacituzumab govitecan (SG). SG was the first ADC approved by the FDA for treatment of TNBC and combines a TROP2-targeted antibody with a topoisomerase 1 (TOP1) inhibitor as cytotoxic payload [27-29]. As a single-agent, SG improves both progression-free and overall survival compared to standard chemotherapy for patients with metastatic TNBC [28, 29]. Notably, it remains unclear whether targeting TROP2 via SG and other ADCs has therapeutic relevance other than as a TOP1 inhibitor delivery mechanism. Addressing the contribution of TROP2 in this context will likely inform future therapeutic combinations incorporating ADCs, including with immune checkpoint inhibitors.

Here, through in vivo loss- and gain-of-function approaches we reveal a specific role for TROP2 in barrier-mediated immune exclusion that drives tumor progression in TNBC. We find that TROP2 is required for tight junction barrier integrity in TNBC, independent of its intracellular signaling domain, thereby enforcing an immune-poor microenvironment and conferring a poor response to immune checkpoint inhibition. This effect can be reversed via TROP2 targeting to enhance response to anti-PD1 therapy in vivo.

RESULTS

Given substantial controversy regarding TROP2 function in cancer, we began with an unbiased approach to define pathways associated with TROP2 expression via analysis of RNAseq data from human breast tumors. We employed Gene Set Variation Analysis (GSVA), an adaptation of Gene set enrichment (GSE) that is robust and highly suited to the inter-patient heterogeneity characteristic of human cancer [30]. An immunity pathway was the most negatively correlated pathway with TROP2 expression in breast cancer, while the pathway most positively associated with TROP2 was tight junctions (Fig. 1A). We therefore hypothesized that TROP2 expression might influence the tumor microenvironment in breast cancer, and next interrogated an independent tumor dataset using TIMER, which infers cell populations from bulk RNAseq [31]. TROP2 expression was strongly inversely correlated with T cell and immune effector genes including PD1 (PDCD1), granzyme (GZMB) and perforin (PRF1), in multiple breast cancer subtypes but most strongly in TNBC (Fig. 1B). We also confirmed that TROP2 was associated with a signature of Tumor Immune Dysfunction and Exclusion (TIDE) in a distinct cohort [9] (Fig. S1A). As it is known that lymphocyte counts are prognostic in TNBC [32, 33], we assessed the association of TROP2 levels with relapse-free, metastasis-free and overall survival in basal-like cancers, which are primarily TNBC. High TROP2 expression in each case predicted poor outcome and short survival (Fig. 1C and Supplementary Fig. S1B, C). Thus, TROP2 is associated with a paucity of T cells and poor outcomes in triple-negative and basal-like breast cancers.

To understand the mechanisms of TROP2 in TNBC we employed multiple TROP2-expressing syngeneic TNBC models. We ablated endogenous TROP2 via CRISPR-Cas-9 (Fig. 1D), then

tested effects in vitro and in vivo through mammary fat pad injection using both immune-deficient and immune-competent hosts. Consistently, loss of TROP2 had no significant effect on proliferation in vitro or on tumor growth in T-cell deficient (nude) mice (Fig. 1E and F, Supplementary Fig. S2A-C). In contrast, TROP2 loss substantially attenuated tumor growth in immune-competent mice compared to control tumors harboring a Cas9/non-targeting gRNA control vector (Fig. 1G and Supplementary Fig. S2D). These data suggest that TROP2 promotes tumor growth in an immune-dependent manner.

Immunohistochemistry analysis revealed few $CD3^+$ T cells in TROP2-expressing tumors (TROP2-WT), whereas TROP2-knockout (TROP2-KO) tumors were more heavily infiltrated (Fig. 2A and B, Supplementary Fig. S2E and S2F). All of these results were consistent across both murine TNBC models (Fig. 1-2 and Supplementary Fig. S2A-F). Using flow cytometry, we then analyzed T cell sub-populations in TROP2-WT and TROP2-KO tumors. We observed significant increases in $CD8^+$ T cell populations including effector memory cells ($CD44^+/CD62L^-$) and activated $PD1^+$ and $Granzyme^+$ cells (Fig. 2C-H) in TROP2-KO tumors. Furthermore, RNAseq analysis of the bulk tumors deconvoluted using CIBERSORT and TIMER consistently demonstrated significant increases in $CD8^+$ cells (Supplementary Fig. S2G). Collectively, these data show that loss of TROP2 results in infiltration of effector memory and activated T cells in association with breast tumor regression.

We then tested directly the contribution of cytotoxic T cells in the setting of TROP2 loss. We carried out IgG-mediated CD8 T cell depletion in mice bearing TROP2-WT or matched TROP2-

KO TNBC tumors (Fig. 2I). In mice treated with control IgG, tumors with loss of TROP2 displayed a substantial growth disadvantage as we had observed previously. However, in the setting of CD8 depletion the difference in growth between TROP2-KO and TROP2-WT tumors was abolished (Fig. 2J). These differences were also reflected in tumor progression and animal survival to a humane endpoint, as loss of TROP2 led to increased survival of IgG-treated mice, whereas survival was not different in mice bearing TROP2-KO vs. TROP2-WT tumors in anti-CD8 treated mice (Fig. 2K). Taken together, these findings support a role for TROP2 in immune cell exclusion of $CD8^+$ effector cells that drives tumor progression.

We next sought to uncover how TROP2 may instigate immune exclusion and to probe the concordance in TROP2-associated pathways between our murine models and human tumors. Thus, we carried out bulk RNAseq analysis of matched TROP2-WT and TROP2-KO tumors and identified altered transcriptional programs via Gene Set Enrichment Analysis (GSEA). Indeed, we observed agreement in signatures associated with TROP2 expression in human and mouse tumors, as the top gene sets positively enriched in TROP2-WT versus TROP2-KO tumors involved cell-cell contact and tight junctions, whereas the most negatively enriched pathways were those involving inflammation, tumor immune responses, and T cell cytotoxicity (Fig. 3A and Supplementary Fig. S3A). The potential association of TROP2 in this context with tight junctions was particularly intriguing, as TROP2 is reported to have a highly tissue-selective role in tight junction formation within the normal corneal epithelium, which is disrupted by germline loss-of-function *TACSTD2* mutations [24]. In the cornea, TROP2 interacts with Claudin 7, a key tight junction protein whose downregulation is known to result in disruption of these structures [26]. Thus, we next tested the physical interaction of TROP2 and Claudin 7, and observed strong

co-immunoprecipitation (co-IP) of the two proteins in both human and murine TNBC cells (Fig. 3B). We then performed immunofluorescence for Claudin 7 in the TROP2-WT and TROP2-KO TNBC tumors. As anticipated, in tumors expressing endogenous TROP2, Claudin 7 showed primarily membrane localization and strong co-localization with TROP2, indicative of intact tight junctions. However, tumors with loss of TROP2 demonstrated substantially decreased expression and abrogated membrane localization of Claudin 7 protein, as well as decreased expression of both Claudin 7 and Claudin 1 mRNA (Fig. 3C, D and Supplementary Fig. S3B). We further probed tight junction integrity through analysis of Occludin, a transmembrane protein that plays a critical role in the barrier function of tight junctions [34, 35]. While TROP2-WT tumors demonstrated strong membrane Occludin staining, TROP2-KO tumors showed dramatic loss of Occludin staining and localization, as well as decreased mRNA expression (Fig. 3E, F and Supplementary Fig. S3B). Notably, Claudin 1, 7 and Occludin expression are all highly positively correlated with TROP2 expression in human breast tumors (Supplementary Fig. S3C). Thus, TROP2 physically interacts with Claudin 7 in TNBC, and its loss disrupts tight junctions via altered expression and localization of multiple integral tight junction proteins.

We next employed reconstitution experiments to establish whether restoration of TROP2 expression was sufficient to mediate immune exclusion and tumor progression. Prior studies have linked TROP2 signaling and function in cancer to its intracellular domain (ICD), whereas binding to Claudin 7 may be mediated through its transmembrane region [36]. Therefore, we tested whether the ICD was required to promote immune exclusion and tumor progression by generating a truncated TROP2 protein containing the extracellular and transmembrane domains (TROP2-ECDTM) but lacking the ICD. We reconstituted TROP2-KO TNBC cells with either

full-length TROP2 or the TROP2-ECDTM truncation mutant, and confirmed by flow cytometry that both proteins were localized to the cell surface (Fig. 4A). We found that indeed the truncated TROP2-ECDTM physically associated with Claudin 7 by co-IP (Supplementary Fig. S3D). Neither full-length TROP2 nor the ECDTM mutant affected tumor cell proliferation compared to TROP-2 KO cells in vitro (Fig. 4B). We then implanted the TROP2-KO or the TROP2 reconstituted cells into syngeneic hosts. TROP2 reconstitution strongly promoted tumor growth in vivo as demonstrated previously, and most importantly reconstitution with TROP2-ECDTM conferred a similar growth advantage (Fig. 4C). TROP2-ECDTM reconstitution fully restored Claudin 7 expression to the level seen in full length TROP2-reconstituted tumors (Fig. 4D and E), and this effect was associated with a substantial decrease in T cell infiltration in reconstituted tumors (Fig. 4F and G). These findings demonstrate that the C-terminal intracellular domain of TROP2 is dispensable for Claudin 7 interaction and expression that are associated with immune exclusion and TNBC progression in vivo.

Based on these findings we sought to therapeutically exploit the role of TROP2 in immune exclusion by testing effects of TROP2 targeting on response to PD1 checkpoint blockade. Sacituzumab govitecan (SG) is a TROP2 directed antibody drug conjugate (ADC) comprised of the hRS7 antibody, whose binding to TROP2 on the cell surface results in its rapid internalization, linked to a topoisomerase 1 inhibitor [37]. To circumvent complications induced by the SG cytotoxic payload-topoisomerase 1 inhibitor, we choose to employ naked hRS7 in combination with PD1 checkpoint blockade. This experiment required reconstitution of TROP2-KO TNBC cells with human TROP2 (hTROP2), as hRS7 does not interact with the murine protein. We first demonstrated that hTROP2 interacted strongly by co-IP with murine Claudin 7

in these cells (Fig. 5A and B). Accordingly, following implantation of cells reconstituted with either control vector or hTROP2 into syngeneic hosts, we observed a significant growth advantage of the hTROP2-expressing tumors (Supplementary Fig. S4A). Furthermore, analogous to the effects of murine TROP2 reconstitution, while TROP2-KO tumors reconstituted with control vector were heavily infiltrated with T cells, hTROP2-reconstitued tumors demonstrated a paucity of T cells throughout the tumor (Supplementary Fig. S4B and C). We then generated larger cohorts of tumor-bearing mice and carried out a 4-arm experiment, treating with control vehicle, hRS7, anti-PD1, or the combination. Single-agent hRS7 did not significantly affect tumor progression, indicating little or no cytotoxic effect of hRS7 alone at doses used. Similarly, anti-PD1 alone had little effect in this relatively poorly immunogenic model. In contrast, the combination of hRS7 and anti-PD1 significantly impeded tumor progression in hTROP2-reconstituted tumors (Fig. 5C). Importantly, immunofluorescence staining and immunohistochemistry showed a significant reduction of Cludin7 and increased $CD3^+$ cells, respectively, in the hRS7-treated tumors compared to vehicle group (Fig. 5D-G), suggesting a disrupted tight junction barrier and increased permeability of immune infiltration. In addition, the anti-PD1 and combination treatment significantly enhanced the proportion of early activated ($TIM3^-CD8^+PD1^+$) $CD8^+$ T cells (Fig. 5H, I). Thus, dual TROP2 targeting and immune checkpoint blockade is superior to either treatment alone in abrogating tumor progression in TNBC. Collectively, our data suggest that both increasing immune accessibility via TROP2 targeting and boosting immune effector function via anti-PD1 are necessary to achieve a significant tumor growth suppression.

Finally, we sought to test the contribution of TROP2 to immunotherapy response in human breast cancer. We identified cohorts with available pre-treatment tumor RNAseq data in which breast cancer patients were treated with anti-PD1 therapy (Pembrolizumab), either with or without chemotherapy (Cohorts 1 and 2, respectively [38, 39]). We examined the impact of TROP2 expression on treatment effect through bulk/pseudo-bulk RNA analysis, plotting the odds ratio (OR) for effect as a function of TROP2. We found that for both cohorts high TROP2 expression was significantly negatively associated with treatment effect (OR for Pembrolizumab/chemotherapy Cohort 1: 0.06, 95% CI 0.0-0.61; OR for Pembrolizumab alone Cohort 2: 0.06, 95% CI 0.01-0.36) (Fig. 6A). In these same datasets, expression of the highly homologous epithelial protein EpCAM was not significantly associated with treatment effect in either cohort, and PD-1 expression was significantly positively associated with effect more strongly in Cohort 2 than Cohort 1 (Fig. 6A). We also took advantage of Cohort 2 single-cell RNAseq (scRNAseq) data to demonstrate that TROP2 expression specifically among epithelial cells was significantly associated with treatment effect (OR: 0.15, 95% CI 0.02-0.84), while again EpCAM was not (Supplementary Fig. S5A-C). In addition, when we analyzed the subset of cells identified as CD8 T cells and stratified the patient tumors by epithelial TROP2 expression, we found that CD8 T cells from tumors with high TROP2 exhibit primarily a naïve signature, while those from tumors with low TROP2 had higher interferon response and cytotoxicity signatures (Fig. 6B). These results comport with our discovery that TROP2 expression promotes a program of T cell exclusion, resulting in diminished immune cell engagement and persistence in a naïve state, while low TROP2 tumors are more accessible to immune cells, resulting in activation and cytotoxicity (Fig. 6C).

DISCUSSION

Our study reveals a heretofore unidentified role of TROP2 expression in cancer, enabling a tight junction (TJ)-based barrier mechanism to exclude T cells and evade anti-tumor immunity. These findings have implications far beyond TROP2 itself, as they underscore a potentially broad role for TJs as a mechanism of barrier-mediated immune exclusion in human cancer. Accordingly, this work suggests the possibility that targeting not only TROP2 but also other tight junction-associated proteins could be fruitfully employed to reverse immune evasion and enhance anti-tumor immunity. Furthermore, although our study focuses on breast cancer, TROP2 is likely to play a similar role in control of TJs, the immune microenvironment and checkpoint blockade response in other tumor types that exhibit aberrant TROP2 expression, including melanoma, ovarian and lung cancers [3, 40].

Notably, we do not observe significant cell-autonomous effects of TROP2 knockout on tumor cell proliferation in vitro or tumor progression in immunodeficient models. Furthermore, we find that reconstitution of knockout cells with a truncated TROP2 mutant lacking the intracellular signaling domain is sufficient to fully restore claudin integrity and tumor growth in vivo. While our findings do not exclude a potential contribution of the TROP2 intracellular domain and its signaling in some contexts, these results highlight for the first time a central role of claudin interaction and TJ-mediated immune exclusion as drivers of tumor progression mediated by TROP2 [15].

The potential ability of TROP2 to control TJ integrity and immune exclusion in multiple cancer types contrasts with the highly tissue-specific corneal TJ dysregulation associated with germline TROP2 mutation [26]. While the precise mechanism of this tissue specificity is not clear, it could possibly be explained by functional redundancy between TROP2 and EpCAM for claudin regulation in non-tumor contexts [41, 42]. In TNBC, we find that loss of TROP2 is sufficient to disrupt claudin expression and localization in vivo, and that claudin is restored by TROP2 reconstitution. Further underscoring the central role of TROP2 for TJ regulation in TNBC, we find that TROP2-KO tumors also display significantly lower Claudin 1/7 and Occludin mRNA than TROP2-WT tumors, potentially mediated by a recently-described positive feedback loop between tight junction barrier dysfunction and inflammation [43].

We show directly that TROP2 impedes tumor infiltration by immune cells in TNBC models, and that loss of TROP2 enables recruitment of key effector memory, $PD1^+$ and activated $CD8^+$ T cell subsets. Correspondingly, we find that blocking TROP2 with the TROP2-directed antibody component of SG sensitizes refractory TNBC tumors to PD1 inhibition in vivo. In addition, this dual TROP2/PD1 blockade promotes both intra-tumoral accessibility and activation of antitumor T cells. Supporting the relevance of our findings in the clinic, we demonstrate that TROP2 levels are a negative predictor of clinical response and clonal T cell expansion for breast cancer patients receiving anti-PD1 therapy, including single-agent Pembrolizumab without chemotherapy. The central function defined herein for TROP2 in TJ-mediated immune exclusion has broad implications for how TROP2-targeted and other ADCs are employed in the future. Multiple tumor types appear to exhibit TROP2-associated immune exclusion, and these would be reasonable candidates for therapeutic testing with emerging ADCs targeting not only TROP2 but

also other TJ components, potentially in combination with immune checkpoint blockade, which is currently under study in breast cancer [44-46]. An immune-mediated effect linked to TROP2/TJ targeting also highlights the potential for the next generation of ADC designs. These could include the possible incorporation of bispecific immune cell engagers, and immune-activating rather than cytotoxic payloads. Finally, the pivotal link exemplified by TROP2 between intercellular junctions as mechanical barriers and anti-tumor immune exclusion opens up additional new opportunities for innovative investigation and therapeutic development in the field of anti-cancer immunity.

METHODS

Cell Lines

Trop2 was knocked out in mouse mammary tumor cell lines 4T1 (MGH Center for Molecular Therapeutics Cell Bank) and AT-3 (Sigma-Aldrich, SCC178) using TROP2 sgRNA CRISPR/Cas9 All-in-One Lentivector set (ABM, 460591140595). A CRISPR/Cas9 vector with non-targeting sgRNA (ABM, K010) was used to generate control *Trop2*-WT cells. In short, lentiviral packaging was performed by cotransfecting HEK293T cells with CRISPR/Cas9 vector and LV-MAX Lentiviral Packaging Mix (Gibco, A43237V) using Lipofectamine2000 (Invitrogen, 11668-019). After 48h, lentivirus-containing medium was collected, filtered, and used to infect the target tumor cell lines. The infected cells were then expanded and selected by puromycin. Human triple negative breast cancer cell lines MDA-MB468 and HCC1806 were obtained from the MGH Center for Molecular Therapeutics Cell Bank.

The mouse TROP2 cDNA was used to generate expressing plasmids (VectorBuilder) carrying full length TROP2 and TROP2 ECDTM truncated version. Control vector carrying same lentiviral elements but without TROP2 sequence was used as control (Stuff). Human TROP2 cDNA was used to generate hTROP2 expressing plasmid (GeneCopoeia), and empty vector (EV) was used as control plasmid. Reconstituted cells were selected using hygromycin to get stably infected pools. Mouse TROP2 expression plasmids used in the rescue experiments all contain silence mutations at the sgRNA-targeting region.

Immunoprecipitation and Immunoblotting

Immunoprecipitation was performed using Pierce Classic Magnetic IP Kit (Thermo Scientific, 88804) with minor modifications. Briefly, 1-3 million cells were lysed with IP lysis buffer including protease/phosphatase inhibitor cocktail (Cell Signaling Technology, 5872) for 10 mins. The lysates were centrifuged at 13,000g for 10 mins at 4 degrees to remove debris. The lysate was precleared with IgG for 3-4h at 4 degrees before the overnight incubation with human TROP2 antibody (Invitrogen, 14-6024-82) or mouse TROP2 (R&D, AF1122). The eluted proteins were analyzed by immunoblotting following standard SDS-PAGE. For regular immunoblotting, cultured cells were washed with ice-cold PBS, lysed with 1X SDS lysis buffer (GenScript, MB01015), and analyzed by standard SDS-PAGE. The primary antibodies include anti-mouse TROP2 (Invitrogen, MA5-29829), anti-human TROP2 (Abcam, ab214488), anti-CLAUDIN7 (Invitrogen, 34-9100), and anti-ACTIN (Cell Signaling Technology, 3700).

In Vivo Tumor Study and Treatment

All animal experiments were approved by the Institutional Animal Care and Use Committee at Mass General Hospital. Eight-week-old female BALB/C (Jackson Laboratory, 000651) and nude (MGH Cox-7 gnotobiotic animal facility) mice were used for in vivo studies. Mice were randomly allocated where appropriate. For antibody and drug treatments, tumors were first measured and randomized into each treatment group to control similar average starting size. 4T1 and AT-3 cells were injected in the mammary fat pad at 0.4-1 × 10^5 cells in 100 μl PBS, unless otherwise stated. Tumors were measured with calipers on the indicated days (volume = 0.5 × length × $width^2$). Tumors were harvested for immunophenotyping by flow cytometry analysis, immunohistochemistry (IHC), or immunofluorescence (IF) at the experiment's end point. Survival curve was determined by tumor volume larger than 1,000 mm^3 or animal death.

For anti-PD1 and hRS7 treatment experiments, 4T1 Trop2 KO+hTROP2 were injected into BALB/C mice and allowed to grow to reach approximately 100 mm^3, the mice were then randomized and allocated to four treatment groups. Isotype control IgG (InVivomab, BE0089), anti-PD1 (InVivomab, BE0146) antibodies and/or hRS7 (Gilead) were injected intraperitoneally twice per week until the end point. The treatment doses were 250 μg/injection for SG and 100 μg/injection for IgG/anti-PD1. Tumor measurements were blinded whenever possible.

For $CD8^+$ T cell depletion, each mouse was administered intraperitoneally 200 μg anti-mouse CD8 (BioxCell, BE0061) or IgG2b isotype control (BioxCell, BE0090) one day before tumor inoculation and twice per week thereafter.

Flow Cytometry Analysis

Single-cell suspensions of tumors were obtained by mincing and passing the tissues through 70 μm filters. Cells were stained with Viability Ghost Dye (Tonbo Biosciences, 13-0870) at 4 °C for 10 mins, followed by anti-CD16/32 blocking (Tonbo Bioscience, 70-0161-U500) at 4 °C for 10 min. For surface proteins, cells were stained with anti-CD45 (BioLegend, 103108), anti-CD3 (BioLegend, 100209), anti-CD8a (BioLegend, 100714), anti-TIM3 (BioLegend, 119703), anti-CD44 (BioLegend, 103041), anti-CD62L (BioLegend, 104410), and anti-PD1 (BD Biosciences, 563059) in FACS buffer (2% FBS in PBS). For cytokine staining, cells were treated with anti-CD3/CD28 (Thermo Fisher, 11452D) at 37 °C overnight and then with BD GolgiPlug (BD Biosciences, 550583) at 37 °C for 5 h. Following surface staining, cells were permeabilized using BD Cytofix/Cytoperm kit (BD Biosciences, 554714), and stained with anti-Granzyme B (Invitrogen, 48-8898-82). All antibodies were used at 1:150 dilution. Cells were

fixed using 1% paraformaldehyde and analyzed by BD FACSAria. Data analysis was done on BD FACSDiva and FlowJo software.

For splenocytes, single cell suspension was obtained in the same manner as tumors. For 4T1 surface TROP2 staining, live cells were directly stained with anti-mouse TROP2 (R&D, FAB1122A).

Immunofluorescence and Immunohistochemistry

Tumor tissues were carefully dissected and embedded in Tissue-Tek optimal cutting temperature compound (OCT, Sakura Finetek USA). 20um tissue section was collected and fixed in 4% PFA (diluted from 16% stock in PBS) for 15 minutes at room temperature. After washing with PBS for 3 times every 5 min to remove OCT and then incubate in blocking solution (5% normal donkey serum, 0.25% Triton X-100 in PBS) for 1h at room temperature, followed by incubation with anti-Claudin7 antibody (1:100 dilution; Invitrogen, 34-9100) and anti-Trop2 antibody (10ug/ul; RD system, AF1122) in blocking solution overnight at 4°C. After proper washing, Alexa Fluor 488-conjugated donkey anti-goat secondary antibody (1:500 diluted in blocking solution) for Trop2 and Alexa Fluor 568-conjugated donkey anti-rabbit secondary antibody (1:500 diluted in blocking solution) for Claudin 7 were applied to the tissue section for 1h at room temperature. After washing with PBS four times, tissue sections were preserved in mounting medium. The specimens were mounted with Vectashield and examined with a Zeiss Imager Z2 confocal microscope with 40× NA 1.40 oil differential interference contrast objective at room temperature (22°C) using Zeiss Zen 2.6 Blue edition software.

For CD3 staining, formalin-fixed paraffin-embedded (FFPE) mouse tumor tissues were cut into 4μm sections for staining. Samples were deparaffinized with xylene and then decloaked. Anti-CD3 (dilution: 1:800; Dako, A0452) antibody was incubated at room temperature for 30 min, followed by incubation with rabbit polymer for 30 mins. The samples were stained with 3,3′-Diaminobenzidine, counterstained with hematoxylin and then lithium carbonate, and dehydrated to xylene. Imaging of the samples was performed on OLYMPUS DP74 microscope. Percentages of CD3-positive cells were quantified using QuPath software (v.0.4.1) (https://qupath.github.io). Tumor margin for $CD3^+$ quantification was defined as a region spanning 250μm on either side of the tumor–stroma border. Staining of tumor Occludin used Occludin (E6B4R) Rabbit mAb (CST, 91131), and the analysis for signal intensity was done using Fiji/ImageJ software (https://fiji.sc/).

For Claudin7 immunofluorescence in Trop2 KO 4T1 rescued with full length or ECDTM TROP2, the staining protocol of FFPE samples was identical. The samples were incubated with anti-Claudin7 antibody (1:50 dilution, Invitrogen, 34-9100) at room temperature for 1h, followed by Alexa Flour 555-conjugated goat ant-rabbit secondary antibody (1:500 dilution in blocking buffer). Imaging of the samples was done on Zeiss Imager Z2 confocal microscope. Quantitation of immunofluorescence was performed using HALO image analysis platform (Indica Labs). Using the Area Quantification FL (v2.3.4) module, intensity thresholds were set globally across all 20x confocal images to identify pixels positive for Claudin7 Alex Fluor 568 fluorescent stain. The percentage of positive pixels out of all pixels within the manually annotated tumor area was determined for each image. The images were manually annotated to exclude staining and imaging artifacts from analysis. Cell segmentation and compartment quantification were performed using the HALO HighPlex FL module, which included nuclear detection with the

default AI algorithm based on DAPI signal. Cell compartments were assigned as “membrane” and “non-membrane”. For each cell, the average intensity of Claudin7 Alexa Fluor 568 signal per compartment was determined. Due to the expected membranous staining of Claudin7, a positivity threshold for each image was set as the median non-membrane signal.

RNA-Seq

RNA sequencing was done using 4T1 *Trop2* WT and KO tumors frozen sections. Total RNA was extracted using RNeasy Plus Mini Kit (Qiagen, 74134). RNA integrity was checked with Agilent 4200 TapeStation System. Following DNA contaminant removal and rRNA depletion, RNA-Seq libraries were constructed using NEBNext Ultra II RNA Library Preparation Kit for Illumina. In brief, RNAs were fragmented at 94°C for 15 min. First and second strand cDNA synthesis was done using primers for random priming sites and Unique Molecular Identifiers (UMIs), which were incorporated into final cDNA. After adapter ligation, cDNAs were purified and enriched by PCR to generate sequencing libraries. RNA-Seq libraries were sequenced using Illumina HiSeq 400 platform, and analysis was done on HiSeq Control Software (HCS). Raw fastq file for each tumor sample was generated by demultiplexing with Illumina bcl2fastq 2.17 software. Gene set enrichment analysis was done using GSEA 4.3.2 software (gsea-msigdb.org).

Bioinformatic analysis

For single cell data processing, original data were retrieved from European Genome-phenome Archive (EGA) and Gene Expression Omnibus (GEO) with data accession no. EGAD00001006608 [39]. SCTransform was used to normalize the data. AggregateData function in

muscat package was used to generate pseudobulk counts for cancer epithelial cells and total immune cells. EdgeR package was used to perform TMM standardization after 0 was removed to generate counts per million (CPM) expression matrix. For bulk RNA-seq analysis in GSE241876 [38], same edgeR based methods as mentioned above for single cell were used to generate CPM expression matrix. For the calculation of Odds Ratios, samples were divided into two groups according to the CPM values of the gene. The OptimalCutpoints package was used to calculate the Youden index to determine the optimal cutoff value, and the logistic regression was then used to generate OR and 95% CI. Non-responsive group (NR) includes progressive disease (PD) and stable disease (SD), and responsive group (R) includes partial responses (PR) and complete responses (CR). T cell receptor clonotype expansion or non-expansion categories were defined by original paper through single-cell T cell receptor (TCR)-seq.

Acknowledgements

We gratefully acknowledge Immunomedics/Gilead for the gift of sacituzumab govitecan. This work was supported by DOD/CDMRP Grant BC200924 and by R01CA260890 (to L.W. Ellisen, A. Bardia), by the Tracey Davis Memorial Breast Cancer Research Fund (to L.W. Ellisen), and by NIH/NCI K99CA286969 and The Terri Brodeur Breast Cancer Foundation Fellowship (to B. Wu).

We thank Grace Dejun Wu, Akiko Suzuki, David Li and MGH Histopathology Research Core for their assistance.

References

1. Stofkova A, Murakami M. Neural activity regulates autoimmune diseases through the gateway reflex. Bioelectron Med. 2019;5:14. Epub 20190820. doi: 10.1186/s42234-019-0030-2. PubMed PMID: 32232103; PMCID: PMC7098223.

2. Fasano A, Shea-Donohue T. Mechanisms of disease: the role of intestinal barrier function in the pathogenesis of gastrointestinal autoimmune diseases. Nat Clin Pract Gastroenterol Hepatol. 2005;2(9):416-22. doi: 10.1038/ncpgasthep0259. PubMed PMID: 16265432.

3. Salerno EP, Bedognetti D, Mauldin IS, Deacon DH, Shea SM, Pinczewski J, Obeid JM, Coukos G, Wang E, Gajewski TF, Marincola FM, Slingluff CL, Jr. Human melanomas and ovarian cancers overexpressing mechanical barrier molecule genes lack immune signatures and have increased patient mortality risk. Oncoimmunology. 2016;5(12):e1240857. Epub 20161018. doi: 10.1080/2162402x.2016.1240857. PubMed PMID: 28123876; PMCID: PMC5215363.

4. Ortiz-Muñoz G, Brown M, Carbone CB, Pechuan-Jorge X, Rouilly V, Lindberg H, Ritter AT, Raghupathi G, Sun Q, Nicotra T, Mantri SR, Yang A, Doerr J, Nagarkar D, Darmanis S, Haley B, Mariathasan S, Wang Y, Gomez-Roca C, de Andrea CE, Spigel D, Wu T, Delamarre L, Schöneberg J, Modrusan Z, Price R, Turley SJ, Mellman I, Moussion C. In situ tumour arrays reveal early environmental control of cancer immunity. Nature. 2023;618(7966):827-33. Epub 20230531. doi: 10.1038/s41586-023-06132-2. PubMed PMID: 37258670; PMCID: PMC10284705.

5. Sun X, Wu B, Chiang HC, Deng H, Zhang X, Xiong W, Liu J, Rozeboom AM, Harris BT, Blommaert E, Gomez A, Garcia RE, Zhou Y, Mitra P, Prevost M, Zhang D, Banik D, Isaacs C, Berry D, Lai C, Chaldekas K, Latham PS, Brantner CA, Popratiloff A, Jin VX, Zhang N, Hu Y, Pujana MA, Curiel TJ, An Z, Li R. Tumour DDR1 promotes collagen fibre alignment to

instigate immune exclusion. Nature. 2021;599(7886):673-8. Epub 20211103. doi: 10.1038/s41586-021-04057-2. PubMed PMID: 34732895; PMCID: PMC8839149.

6. Hegde PS, Chen DS. Top 10 Challenges in Cancer Immunotherapy. Immunity. 2020;52(1):17-35. doi: 10.1016/j.immuni.2019.12.011. PubMed PMID: 31940268.

7. Gruosso T, Gigoux M, Manem VSK, Bertos N, Zuo D, Perlitch I, Saleh SMI, Zhao H, Souleimanova M, Johnson RM, Monette A, Ramos VM, Hallett MT, Stagg J, Lapointe R, Omeroglu A, Meterissian S, Buisseret L, Van den Eynden G, Salgado R, Guiot MC, Haibe-Kains B, Park M. Spatially distinct tumor immune microenvironments stratify triple-negative breast cancers. J Clin Invest. 2019;129(4):1785-800. Epub 20190318. doi: 10.1172/jci96313. PubMed PMID: 30753167; PMCID: PMC6436884.

8. Wang K, Xu J, Zhang T, Xue D. Tumor-infiltrating lymphocytes in breast cancer predict the response to chemotherapy and survival outcome: A meta-analysis. Oncotarget. 2016;7(28):44288-98. doi: 10.18632/oncotarget.9988. PubMed PMID: 27329588; PMCID: PMC5190096.

9. Jiang P, Gu S, Pan D, Fu J, Sahu A, Hu X, Li Z, Traugh N, Bu X, Li B, Liu J, Freeman GJ, Brown MA, Wucherpfennig KW, Liu XS. Signatures of T cell dysfunction and exclusion predict cancer immunotherapy response. Nat Med. 2018;24(10):1550-8. Epub 20180820. doi: 10.1038/s41591-018-0136-1. PubMed PMID: 30127393; PMCID: PMC6487502.

10. Cheng CY, Wong EW, Lie PP, Li MW, Mruk DD, Yan HH, Mok KW, Mannu J, Mathur PP, Lui WY, Lee WM, Bonanomi M, Silvestrini B. Regulation of blood-testis barrier dynamics by desmosome, gap junction, hemidesmosome and polarity proteins: An unexpected turn of events. Spermatogenesis. 2011;1(2):105-15. doi: 10.4161/spmg.1.2.15745. PubMed PMID: 22319658; PMCID: PMC3271652.

11. Mohan KV, Mishra A, Muniyasamy A, Sinha P, Sahu P, Kesarwani A, Jain K, Nagarajan P, Scaria V, Agarwal M, Akhter NS, Gupta C, Upadhyay P. Immunological consequences of compromised ocular immune privilege accelerate retinal degeneration in retinitis pigmentosa. Orphanet J Rare Dis. 2022;17(1):378. Epub 20221017. doi: 10.1186/s13023-022-02528-x. PubMed PMID: 36253797; PMCID: PMC9575261.

12. Smith BE, Braun RE. Germ cell migration across Sertoli cell tight junctions. Science. 2012;338(6108):798-802. Epub 20120920. doi: 10.1126/science.1219969. PubMed PMID: 22997133; PMCID: PMC3694388.

13. Zaman S, Jadid H, Denson AC, Gray JE. Targeting Trop-2 in solid tumors: future prospects. Onco Targets Ther. 2019;12:1781-90. Epub 20190301. doi: 10.2147/ott.S162447. PubMed PMID: 30881031; PMCID: PMC6402435.

14. Ambrogi F, Fornili M, Boracchi P, Trerotola M, Relli V, Simeone P, La Sorda R, Lattanzio R, Querzoli P, Pedriali M, Piantelli M, Biganzoli E, Alberti S. Trop-2 is a determinant of breast cancer survival. PLoS One. 2014;9(5):e96993. Epub 20140513. doi: 10.1371/journal.pone.0096993. PubMed PMID: 24824621; PMCID: PMC4019539.

15. Lenárt S, Lenárt P, Šmarda J, Remšík J, Souček K, Beneš P. Trop2: Jack of All Trades, Master of None. Cancers (Basel). 2020;12(11). Epub 20201111. doi: 10.3390/cancers12113328. PubMed PMID: 33187148; PMCID: PMC7696911.

16. Lin JC, Wu YY, Wu JY, Lin TC, Wu CT, Chang YL, Jou YS, Hong TM, Yang PC. TROP2 is epigenetically inactivated and modulates IGF-1R signalling in lung adenocarcinoma. EMBO Mol Med. 2012;4(6):472-85. Epub 20120315. doi: 10.1002/emmm.201200222. PubMed PMID: 22419550; PMCID: PMC3443948.

17. Li X, Teng S, Zhang Y, Zhang W, Zhang X, Xu K, Yao H, Yao J, Wang H, Liang X, Hu Z. TROP2 promotes proliferation, migration and metastasis of gallbladder cancer cells by regulating PI3K/AKT pathway and inducing EMT. Oncotarget. 2017;8(29):47052-63. doi: 10.18632/oncotarget.16789. PubMed PMID: 28423362; PMCID: PMC5564543.

18. Cubas R, Zhang S, Li M, Chen C, Yao Q. Trop2 expression contributes to tumor pathogenesis by activating the ERK MAPK pathway. Mol Cancer. 2010;9:253. Epub 20100921. doi: 10.1186/1476-4598-9-253. PubMed PMID: 20858281; PMCID: PMC2946292.

19. Hou J, Lv A, Deng Q, Zhang G, Hu X, Cui H. TROP2 promotes the proliferation and metastasis of glioblastoma cells by activating the JAK2/STAT3 signaling pathway. Oncol Rep. 2019;41(2):753-64. Epub 20181109. doi: 10.3892/or.2018.6859. PubMed PMID: 30431125; PMCID: PMC6312989.

20. Stoyanova T, Goldstein AS, Cai H, Drake JM, Huang J, Witte ON. Regulated proteolysis of Trop2 drives epithelial hyperplasia and stem cell self-renewal via β-catenin signaling. Genes Dev. 2012;26(20):2271-85. doi: 10.1101/gad.196451.112. PubMed PMID: 23070813; PMCID: PMC3475800.

21. Alavi A, Elahi E, Tehrani MH, Amoli FA, Javadi MA, Rafati N, Chiani M, Banihosseini SS, Bayat B, Kalhor R, Amini SS. Four mutations (three novel, one founder) in TACSTD2 among Iranian GDLD patients. Invest Ophthalmol Vis Sci. 2007;48(10):4490-7. doi: 10.1167/iovs.07-0264. PubMed PMID: 17898270.

22. Masmali A, Alkanaan A, Alkatan HM, Kirat O, Almutairi AA, Almubrad T, Akhtar S. Clinical and Ultrastructural Studies of Gelatinous Drop-Like Corneal Dystrophy (GDLD) of a Patient with TACSTD2 Gene Mutation. J Ophthalmol. 2019;2019:5069765. Epub 20190820. doi: 10.1155/2019/5069765. PubMed PMID: 31534795; PMCID: PMC6724435.

23. Quantock AJ, Nishida K, Kinoshita S. Histopathology of recurrent gelatinous drop-like corneal dystrophy. Cornea. 1998;17(2):215-21. doi: 10.1097/00003226-199803000-00018. PubMed PMID: 9520202.

24. Tsujikawa M, Kurahashi H, Tanaka T, Nishida K, Shimomura Y, Tano Y, Nakamura Y. Identification of the gene responsible for gelatinous drop-like corneal dystrophy. Nat Genet. 1999;21(4):420-3. doi: 10.1038/7759. PubMed PMID: 10192395.

25. Takaoka M, Nakamura T, Ban Y, Kinoshita S. Phenotypic investigation of cell junction-related proteins in gelatinous drop-like corneal dystrophy. Invest Ophthalmol Vis Sci. 2007;48(3):1095-101. doi: 10.1167/iovs.06-0740. PubMed PMID: 17325151.

26. Nakatsukasa M, Kawasaki S, Yamasaki K, Fukuoka H, Matsuda A, Tsujikawa M, Tanioka H, Nagata-Takaoka M, Hamuro J, Kinoshita S. Tumor-associated calcium signal transducer 2 is required for the proper subcellular localization of claudin 1 and 7: implications in the pathogenesis of gelatinous drop-like corneal dystrophy. Am J Pathol. 2010;177(3):1344-55. Epub 20100722. doi: 10.2353/ajpath.2010.100149. PubMed PMID: 20651236; PMCID: PMC2928967.

27. Coates JT, Sun S, Leshchiner I, Thimmiah N, Martin EE, McLoughlin D, Danysh BP, Slowik K, Jacobs RA, Rhrissorrakrai K, Utro F, Levovitz C, Denault E, Walmsley CS, Kambadakone A, Stone JR, Isakoff SJ, Parida L, Juric D, Getz G, Bardia A, Ellisen LW. Parallel Genomic Alterations of Antigen and Payload Targets Mediate Polyclonal Acquired Clinical Resistance to Sacituzumab Govitecan in Triple-Negative Breast Cancer. Cancer Discov. 2021;11(10):2436-45. Epub 20210817. doi: 10.1158/2159-8290.Cd-21-0702. PubMed PMID: 34404686; PMCID: PMC8495771.

28. Bardia A, Mayer IA, Vahdat LT, Tolaney SM, Isakoff SJ, Diamond JR, O'Shaughnessy J, Moroose RL, Santin AD, Abramson VG, Shah NC, Rugo HS, Goldenberg DM, Sweidan AM, Iannone R, Washkowitz S, Sharkey RM, Wegener WA, Kalinsky K. Sacituzumab Govitecan-hziy in Refractory Metastatic Triple-Negative Breast Cancer. N Engl J Med. 2019;380(8):741-51. doi: 10.1056/NEJMoa1814213. PubMed PMID: 30786188.

29. Bardia A, Hurvitz SA, Tolaney SM, Loirat D, Punie K, Oliveira M, Brufsky A, Sardesai SD, Kalinsky K, Zelnak AB, Weaver R, Traina T, Dalenc F, Aftimos P, Lynce F, Diab S, Cortés J, O'Shaughnessy J, Diéras V, Ferrario C, Schmid P, Carey LA, Gianni L, Piccart MJ, Loibl S, Goldenberg DM, Hong Q, Olivo MS, Itri LM, Rugo HS. Sacituzumab Govitecan in Metastatic Triple-Negative Breast Cancer. N Engl J Med. 2021;384(16):1529-41. doi: 10.1056/NEJMoa2028485. PubMed PMID: 33882206.

30. Hänzelmann S, Castelo R, Guinney J. GSVA: gene set variation analysis for microarray and RNA-seq data. BMC Bioinformatics. 2013;14:7. Epub 20130116. doi: 10.1186/1471-2105-14-7. PubMed PMID: 23323831; PMCID: PMC3618321.

31. Li T, Fu J, Zeng Z, Cohen D, Li J, Chen Q, Li B, Liu XS. TIMER2.0 for analysis of tumor-infiltrating immune cells. Nucleic Acids Res. 2020;48(W1):W509-w14. doi: 10.1093/nar/gkaa407. PubMed PMID: 32442275; PMCID: PMC7319575.

32. Koh SB, Ellisen LW. Immune activation and evolution through chemotherapy plus checkpoint blockade in triple-negative breast cancer. Cancer Cell. 2021;39(12):1562-4. Epub 20211111. doi: 10.1016/j.ccell.2021.11.001. PubMed PMID: 34767761.

33. Gao G, Wang Z, Qu X, Zhang Z. Prognostic value of tumor-infiltrating lymphocytes in patients with triple-negative breast cancer: a systematic review and meta-analysis. BMC Cancer.

2020;20(1):179. Epub 20200304. doi: 10.1186/s12885-020-6668-z. PubMed PMID: 32131780; PMCID: PMC7057662.

34. Horowitz A, Chanez-Paredes SD, Haest X, Turner JR. Paracellular permeability and tight junction regulation in gut health and disease. Nat Rev Gastroenterol Hepatol. 2023;20(7):417-32. Epub 20230425. doi: 10.1038/s41575-023-00766-3. PubMed PMID: 37186118; PMCID: PMC10127193.

35. Sugiyama S, Sasaki T, Tanaka H, Yan H, Ikegami T, Kanki H, Nishiyama K, Beck G, Gon Y, Okazaki S, Todo K, Tamura A, Tsukita S, Mochizuki H. The tight junction protein occludin modulates blood-brain barrier integrity and neurological function after ischemic stroke in mice. Sci Rep. 2023;13(1):2892. Epub 20230218. doi: 10.1038/s41598-023-29894-1. PubMed PMID: 36806348; PMCID: PMC9938878.

36. Nübel T, Preobraschenski J, Tuncay H, Weiss T, Kuhn S, Ladwein M, Langbein L, Zöller M. Claudin-7 regulates EpCAM-mediated functions in tumor progression. Mol Cancer Res. 2009;7(3):285-99. Epub 20090310. doi: 10.1158/1541-7786.Mcr-08-0200. PubMed PMID: 19276185.

37. Shih LB, Xuan H, Aninipot R, Stein R, Goldenberg DM. In vitro and in vivo reactivity of an internalizing antibody, RS7, with human breast cancer. Cancer Res. 1995;55(23 Suppl):5857s-63s. PubMed PMID: 7493360.

38. Wilkerson AD, Parthasarathy PB, Stabellini N, Mitchell C, Pavicic PG, Jr., Fu P, Rupani A, Husic H, Rayman PA, Swaidani S, Abraham J, Budd GT, Moore H, Al-Hilli Z, Ko JS, Baar J, Chan TA, Alban T, Diaz-Montero CM, Montero AJ. Phase II Clinical Trial of Pembrolizumab and Chemotherapy Reveals Distinct Transcriptomic Profiles by Radiologic Response in

Metastatic Triple-Negative Breast Cancer. Clin Cancer Res. 2024;30(1):82-93. doi: 10.1158/1078-0432.Ccr-23-1349. PubMed PMID: 37882661; PMCID: PMC10767305.

39. Bassez A, Vos H, Van Dyck L, Floris G, Arijs I, Desmedt C, Boeckx B, Vanden Bempt M, Nevelsteen I, Lambein K, Punie K, Neven P, Garg AD, Wildiers H, Qian J, Smeets A, Lambrechts D. A single-cell map of intratumoral changes during anti-PD1 treatment of patients with breast cancer. Nat Med. 2021;27(5):820-32. Epub 20210506. doi: 10.1038/s41591-021-01323-8. PubMed PMID: 33958794.

40. Bessede A, Peyraud F, Besse B, Cousin S, Cabart M, Chomy F, Rey C, Lara O, Odin O, Nafia I, Vanhersecke L, Barlesi F, Guégan JP, Italiano A. TROP2 is associated with primary resistance to immune checkpoint inhibition in patients with advanced non-small cell lung cancer. Clin Cancer Res. 2023. Epub 20231201. doi: 10.1158/1078-0432.Ccr-23-2566. PubMed PMID: 38048058.

41. Szabo R, Ward JM, Artunc F, Bugge TH. EPCAM and TROP2 share a role in claudin stabilization and development of intestinal and extraintestinal epithelia in mice. Biol Open. 2022;11(7). Epub 20220711. doi: 10.1242/bio.059403. PubMed PMID: 35730316; PMCID: PMC9294608.

42. Wu CJ, Lu M, Feng X, Nakato G, Udey MC. Matriptase Cleaves EpCAM and TROP2 in Keratinocytes, Destabilizing Both Proteins and Associated Claudins. Cells. 2020;9(4). Epub 20200421. doi: 10.3390/cells9041027. PubMed PMID: 32326212; PMCID: PMC7226414.

43. Bhat AA, Uppada S, Achkar IW, Hashem S, Yadav SK, Shanmugakonar M, Al-Naemi HA, Haris M, Uddin S. Tight Junction Proteins and Signaling Pathways in Cancer and Inflammation: A Functional Crosstalk. Front Physiol. 2018;9:1942. Epub 20190123. doi: 10.3389/fphys.2018.01942. PubMed PMID: 30728783; PMCID: PMC6351700.

44. Tolaney S, De Azambuja E, Emens L, Loi S, Pan W, Huang J, Sun S, Lai C, Schmid P. 276TiP ASCENT-04/KEYNOTE-D19: Phase III study of sacituzumab govitecan (SG) plus pembrolizumab (pembro) vs treatment of physician's choice (TPC) plus pembro in first-line (1L) programmed death-ligand 1-positive (PD-L1+) metastatic triple-negative breast cancer (mTNBC). Annals of Oncology. 2022;33:S664-S5.

45. Garrido-Castro AC, Keenan TE, Li T, Lange P, Callahan C, Guerriero J, Tayob N, Anderson L, Yam C, Daniel BR. Saci-IO TNBC: Randomized phase II trial of sacituzumab govitecan (SG)+/-pembrolizumab in PD-L1–metastatic triple-negative breast cancer (mTNBC). Wolters Kluwer Health; 2021.

46. Nederlof I, Voorwerk L, Kok M. Facts and Hopes in Immunotherapy for Early-Stage Triple-Negative Breast Cancer. Clin Cancer Res. 2023;29(13):2362-70. doi: 10.1158/1078-0432.Ccr-22-0701. PubMed PMID: 36622327; PMCID: PMC10320476.

Figure Legends

Figure 1. TROP2 promotes mammary tumor growth and immune exclusion in immunocompetent hosts. A, Top 20 pathways positively (blue) or negatively (green) associated with TROP2 expression in human breast cancer identified by Gene Set Variation Analysis (GSVA) using METABRIC dataset. Top and bottom quartiles of TROP2 expression were used to compute the association. **B,** Correlation between TROP2 and immune cell markers in multiple cancer types by TIMER analysis in the TCGA database. Red dashed box indicates breast cancers. **C,** TROP2 predicts poor overall survival in basal subtype of breast cancer. Generated by Kaplan-Meier Plotter database (https://kmplot.com/analysis/). **D,** Western blot for TROP2 in wildtype (WT) and *Trop2* knockout (KO) 4T1 cells. **E-G,** WT and KO 4T1 tumor cell growth in cell culture (E); in immunocompromised (nude) hosts (n = 10 tumors per group) (F), and in syngeneic immunocompetent BALB/C hosts (WT, n = 12 tumors; KO, n = 10 tumors) (G).

Figure 2. TROP2 promotes mammary tumor immune exclusion. A and **B,** Representative images (A) and quantification (B) of $CD3^+$ T cell IHC staining in WT and KO tumor margins and cores. **C** and **D**, Representative flow cytometry contour plots (C) and quantification (D) of $CD44^+CD62L^-$ effector memory $CD8^+$ T cells in WT and KO tumors. **E** and **F**, Representative flow cytometry contour plots (E) and quantification (F) of $PD1^+$ activated $CD8^+$ T cells in WT and KO tumors. **G** and **H**, Representative flow cytometry histogram (G) and quantification (H) of Granzyme B mean fluorescence intensity (MFI) in $CD8^+$ T cells in WT and KO tumors. **I,** Percentages of $CD8^+$ cells among $CD3^+$ T cells in splenocytes harvested from mice treated with control IgG or anti-CD8 depleting antibodies. **J,** *Trop2*-WT and -KO 4T1 tumor growth curves in BALB/C mice treated with control IgG or anti-CD8 depleting antibodies (WT, n = 10 tumors per group; KO/IgG, n = 8 tumors; KO/anti-CD8: n = 6 tumors). **K,** Kaplan-Meier survival curves of WT and KO tumor-bearing BALB/C mice treated with control IgG or anti-CD8 depleting antibodies (WT, n = 10 mice per group; KO/IgG, n = 9 mice; KO/anti-CD8: n = 8 mice).

Figure 3. TROP2 promotes a tight junction-mediated barrier and inhibits a pro-inflammatory tumor immune microenvironment. A, Enriched pathways from Gene set enrichment analysis (GSEA) on bulk RNA-seq of *Trop2*-WT and KO 4T1 tumors harvested from BALB/C hosts. **B,** Western blot analysis showing co-immunoprecipitation (co-IP) of Claudin7 and TROP2 using IgG or anti-TROP2 in *Trop2*-WT and KO 4T1 (left panel), MDA-MB468 (middle panel), and HCC1806 (right panel) TNBC cells. **C,** Representative tumor tissue immunofluorescence images of TROP2, tight junction molecule Claudin7, and DAPI (nuclear stain), showing TROP2/Claudin 7 co-localization, and loss of Claudin7 expression and membrane localization with TROP2 knockout. **D,** Quantification of proportion of membrane Claudin7-expressing cells in WT and KO 4T1 tumors for panel C. **E,** Representative tumor tissue immunofluorescence images of Occludin and DAPI (nuclear stain) showing loss of Occludin expression with TROP2 knockout. **F,** Quantification of Occludin intensity in WT and KO 4T1 tumors for panel E.

Figure 4. TROP2 intracellular domain is dispensable for its tight junction and immune barrier function. A, Histogram showing flow cytometry analysis of cell-surface TROP2 in *Trop2*-KO 4T1 reconstituted with control vector (Stuff), Full-Length TROP2, or C-terminal truncated ECDTM mutant. **B,** In vitro proliferation of *Trop2*-KO 4T1 reconstituted with control vector, Full-Length TROP2 or ECDTM truncated mutant. **C,** Tumor growth curves of *Trop2*-KO 4T1 reconstituted with control vector (Stuff), Full-Length TROP2, or C-terminal truncated ECDTM TROP2 mutant in BALB/C immunocompetent hosts (n = 10 tumors per group). **D,** Representative tumor tissue immunofluorescence images of Claudin7 in tumors harvested from panel C. **E,** Quantification of Claudin7 for panel D. **F** and **G**, Representative images (F) and quantification (G) of $CD3^+$ T cell IHC staining in tumors harvested from panel C.

Figure 5. TROP2 targeting via the naked anti-TROP2 antibody of SG promotes anti-PD1 efficacy. A, Western blot of *Trop2*-KO 4T1 cells reconstituted with empty vector (EV) or human TROP2 (hTROP2). **B,** Western blot showing co-IP of hTROP2 and Claudin 7 in *Trop2*-KO 4T1 cells reconstituted with hTROP2. **C,** Tumor growth curves for KO+hTROP2 (hRS7+anti-PD1, n = 10 tumors; n = 8 tumors per group for other three groups) in BALB/C mice treated with

Vehicle, hRS7, anti-PD1, or hRS7+anti-PD1 combination. Treatment started when tumors reached 100 mm^3. Arrows indicate treatment days. **D,** Representative tumor tissue immunofluorescence images of Claudin7 in tumors harvested from panel C. **E,** Quantification of Claudin7 for panel D. **F** and **G**, Representative images (F) and quantification (G) of $CD3^+$ T cell IHC staining in tumors harvested from panel C. **H** and **I,** Representative flow cytometry contour plots (F) and quantification (G) of $TIM3^-$ early activated $CD8^+PD1^+$ T cells in tumors harvested from panel C. **p*<0.05, ***p*<0.01.

Figure 6. High TROP2 associates with non-responses to immune checkpoint inhibitors in human breast cancers. A, Odds ratios for associations between gene expression (PDCD1 (PD1), TACSTD2 (TROP2) and EPMCAM) and response to anti-PD1 therapy. Cohort 1: Response (evaluated radiologically using RECIST criteria) to combination Pembrolizumab, Carboplatin, and Nab-paclitaxel among patients with advanced TNBC [38]; NR: non-responsive, R: responsive. Cohort 2: Response assessed by T cell receptor clonotype expansion following pre-operative single-agent Pembrolizumab for breast cancer [39], NE: no clonotype expansion, E: yes clonotype expansion. **B,** Violin plots derived from single-cell RNAseq data from the cohort in (A), showing subset signature scores among $CD8^+$ T cells in tumors expressing low vs. high epithelial TROP2 [39]. CD8 signatures are derived from PMID: 37248301. **C,** Proposed model for TROP2-mediated immune exclusion in breast cancer. Left, TROP2 enables a claudin/tight junction-mediated mechanical barrier to exclude antitumor immune infiltration. Right, genetic deletion or pharmacological blockade of TROP2 deregulates the tight junction-mediated mechanical barrier and allows antitumor immune infiltration.

Supplementary Figure Legends

Supplementary Figure S1. A, Correlation between TROP2 and cytotoxic T lymphocyte score (CTL) in GSE10885 dataset by TIDE analysis. **B** and **C,** Correlation between TROP2 and relapse free survival (B) or distant metastasis free survival (C) in basal subtype of breast cancer, generated by Kaplan-Meier Plotter database (https://kmplot.com/analysis/).

Supplementary Figure S2. A, Western blot for wildtype (WT) and *Trop-2* knockout (KO) AT-3 cells. **B-D,** *Trop2*-WT and -KO AT-3 tumor growth curves during in vitro cell culture (B), in immunocompromised (nude) hosts (WT, n = 4 tumors; KO, n = 3 tumors) (C), and in immunocompetent C57BL/6 (BL6) hosts (WT, n = 6 tumors; KO, n = 4 tumors) (D). **E** and **F,** Representative images (E) and quantification (F) of $CD3^+$ T cell IHC staining of WT and KO AT-3 tumor margins and cores. **G,** Computational deconvolution of tumor-infiltrating immune subsets from bulk RNAseq of WT and KO 4T1 tumors using CIBERSORT (left panel) and TIMER algorithm (right panel). Red boxes highlight significant differences in $CD8^+$ T cell populations.

Supplementary Figure S3. A, Gene set enrichment analysis of bulk RNA-seq from *Trop2*-WT and -KO 4T1 tumors (blue asterisk: positive NES; red asterisk: negative NES). **B,** Gene expression (normalized gene counts) for Claudin-7 (*Cldn7*), Claudin-1 (*Cldn1*), and Occludin (*Ocln*) from RNAseq of WT and KO tumors. **C,** Correlation between TROP2 and CLDN1/CLDN7/OCLN expression in basal breast cancer patient cohorts by TIMER analysis using TCGA database. **D,** Western blot showing co-IP of TROP2 and Claudin 7 using IgG and anti-TROP2 in *Trop2*-KO 4T1 reconstituted with Stuff, Full-Length TROP2, or ECDTM truncated mutant. FL: full length.

Supplementary Figure S4. A, Tumor growth curves for KO+EV and KO+hTROP2 4T1 in BALB/C mice (KO+EV, n = 6 tumors; KO+hTROP2, n = 8 tumors). **B** and **C,** Representative

images (B) and quantification (C) of $CD3^+$ T cell IHC staining of KO+EV and KO+hTROP2 tumor margins and cores.

Supplementary Figure S5. A, PDCD1 (PD1), TACSTD2 (TROP2) and EPCAM expression derived from pseudobulk analysis of single-cell RNAseq data in TCR clonotype expanded (E) vs. non-expanded (NE) cases following pre-operative single-agent pembrolizumab [39]. **B,** Gene expression as in (A) from bulk RNAseq in responsive (R) vs. non-responsive (NR) cases following Pembrolizumab, Carboplatin, and Nab-paclitaxel [38]. **C,** Odds ratios for associations between gene expression within the epithelial cell populations and responses (E vs. NE) in the Cohort in (A). *p<0.05, **p<0.01.

Fig. 1 TROP2 promotes mammary tumor growth in immunocompetent hosts.

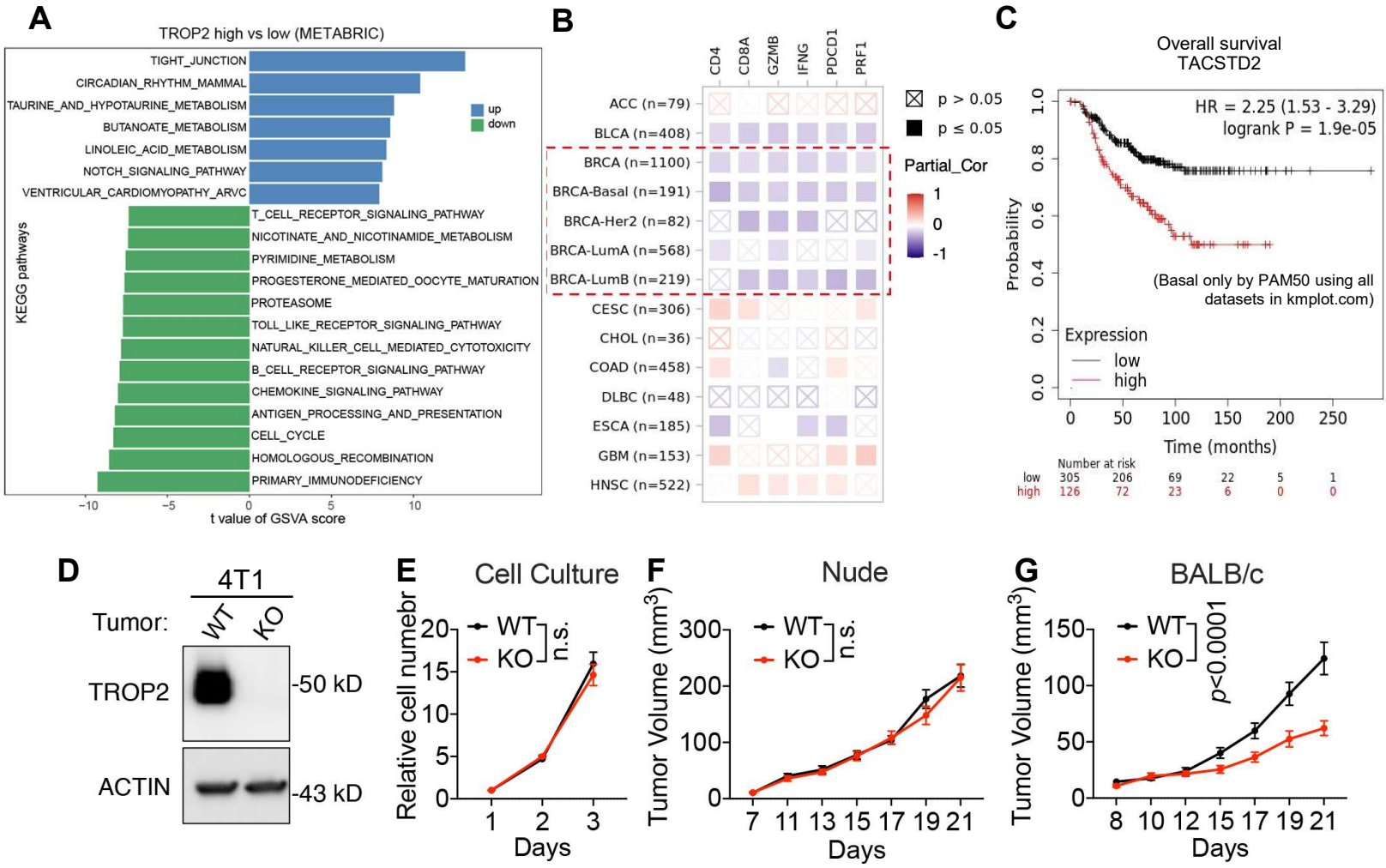

Fig. 2 TROP2 promotes mammary tumor immune exclusion

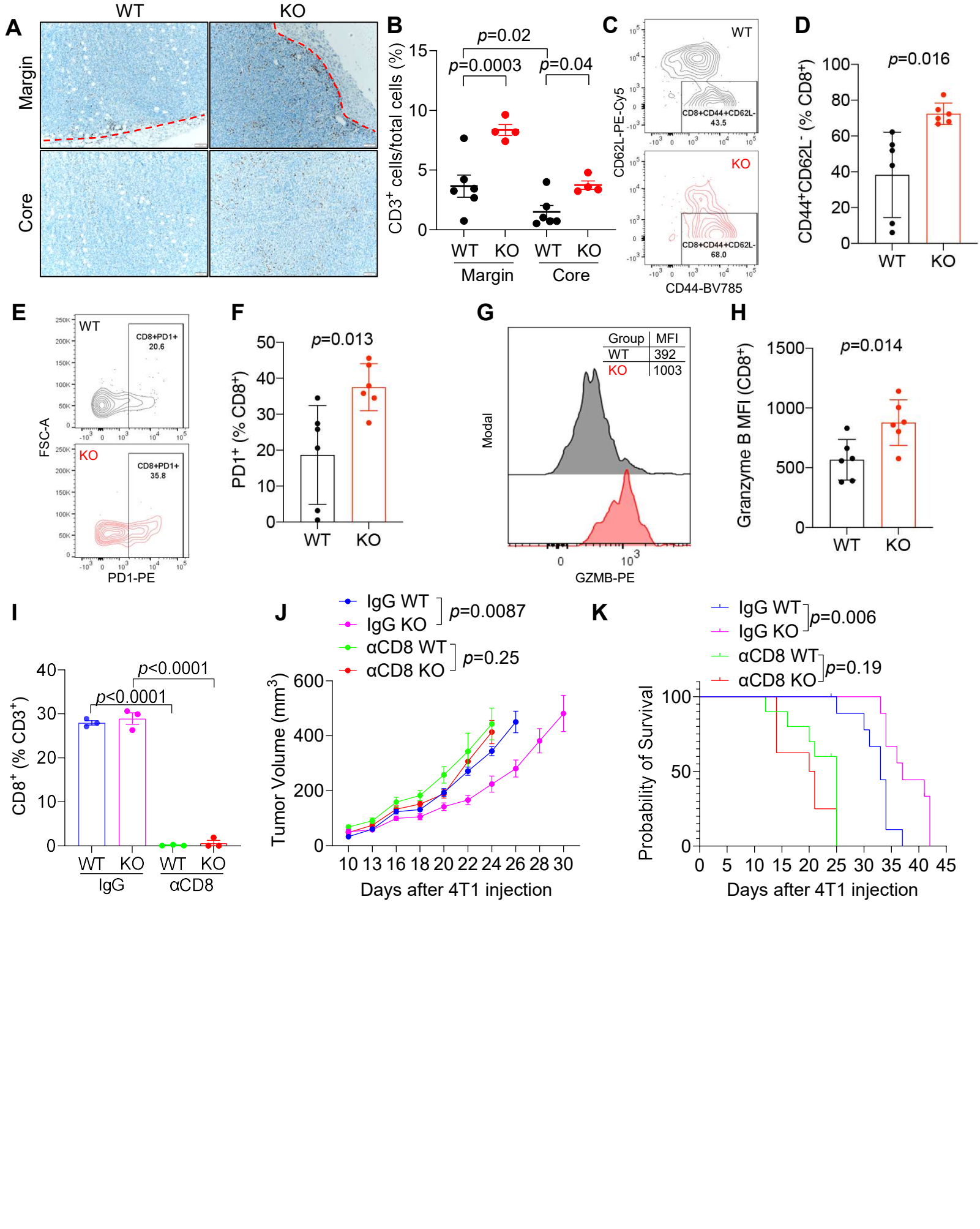

Fig. 3 TROP2 promotes a tight junction-mediated barrier and inhibits a pro-inflammatory tumor immune microenvironment

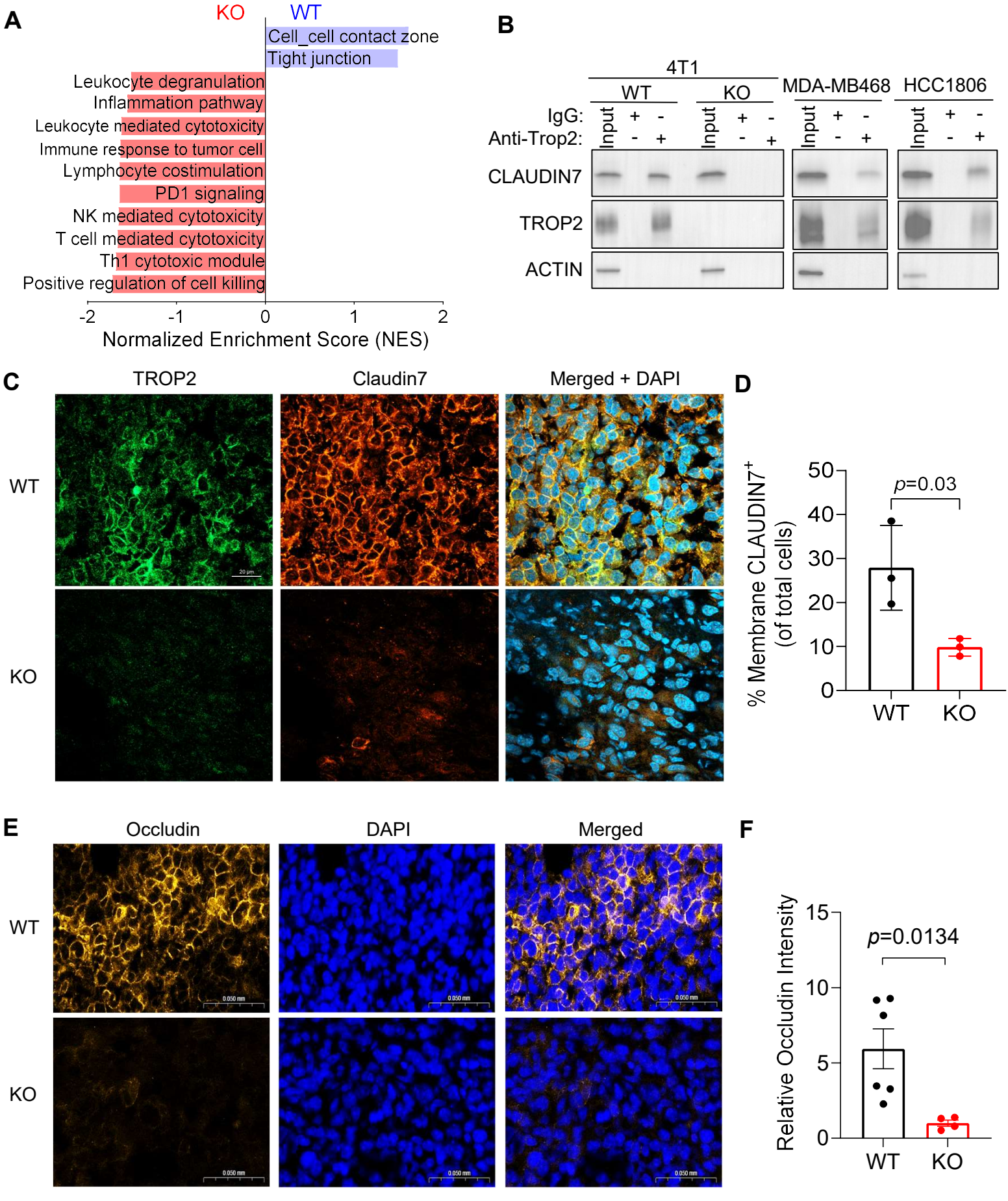

Fig. 4 TROP2 intracellular domain is dispensable for its tight function and immune barrier function

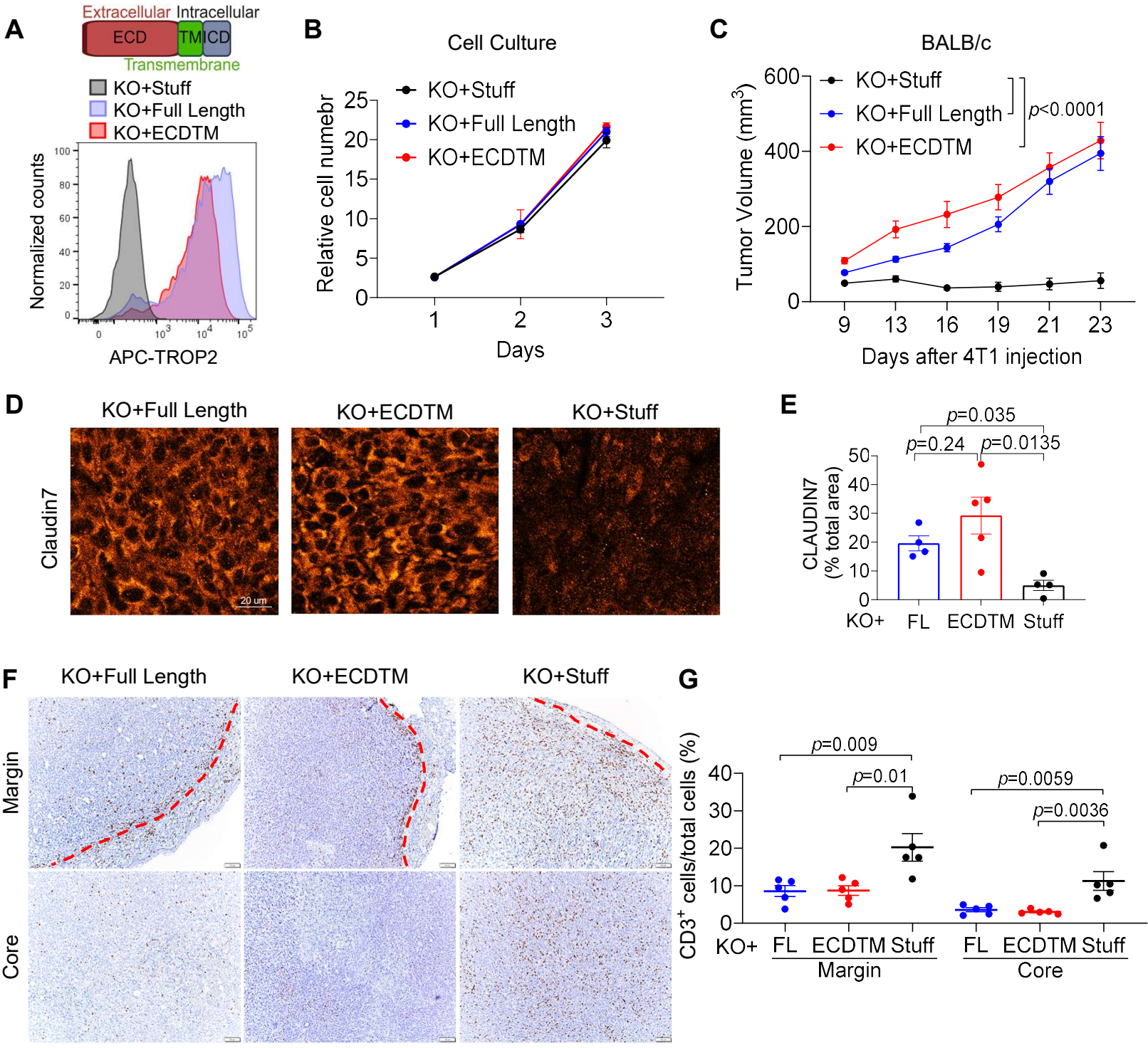

Fig. 5 TROP2 targeting via the naked anti-TROP2 antibody of SG promotes anti-PD1 efficacy

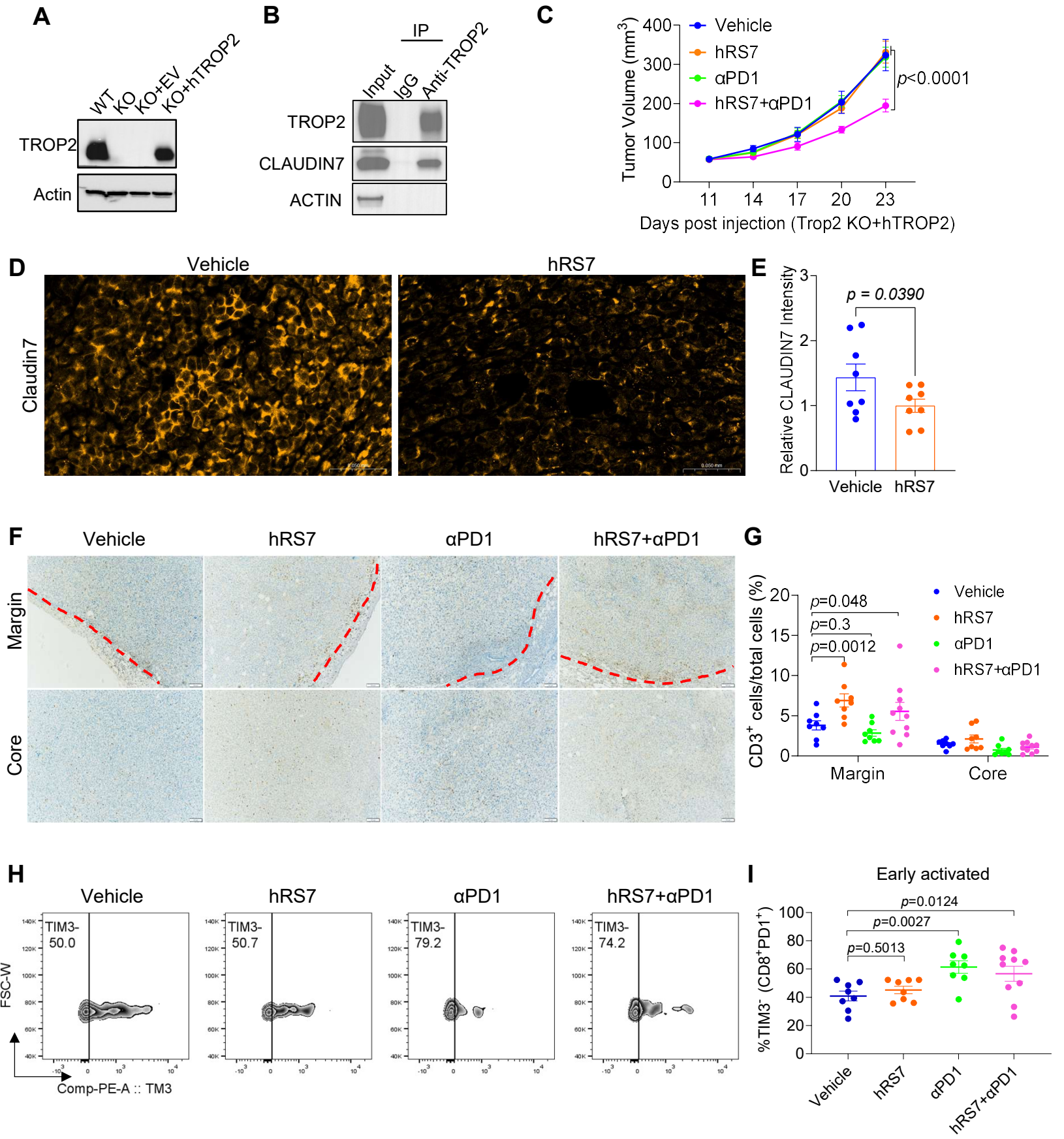

Fig. 6 High TROP2 associates with non-responses to immune checkpoint inhibitors in human breast cancers

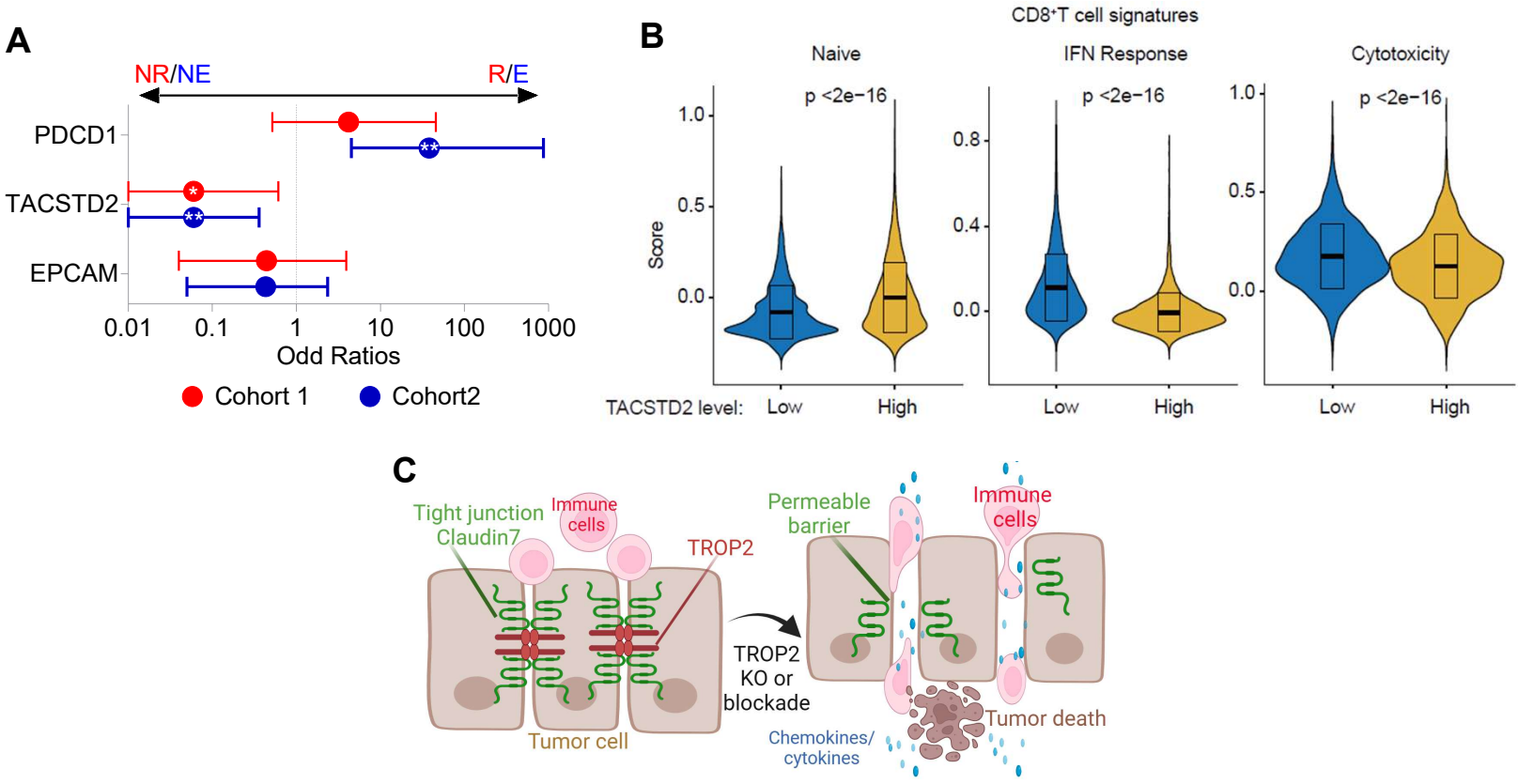

Supplemental Figure S1. High *TACSTD2* associates with cold TME and worse survivals

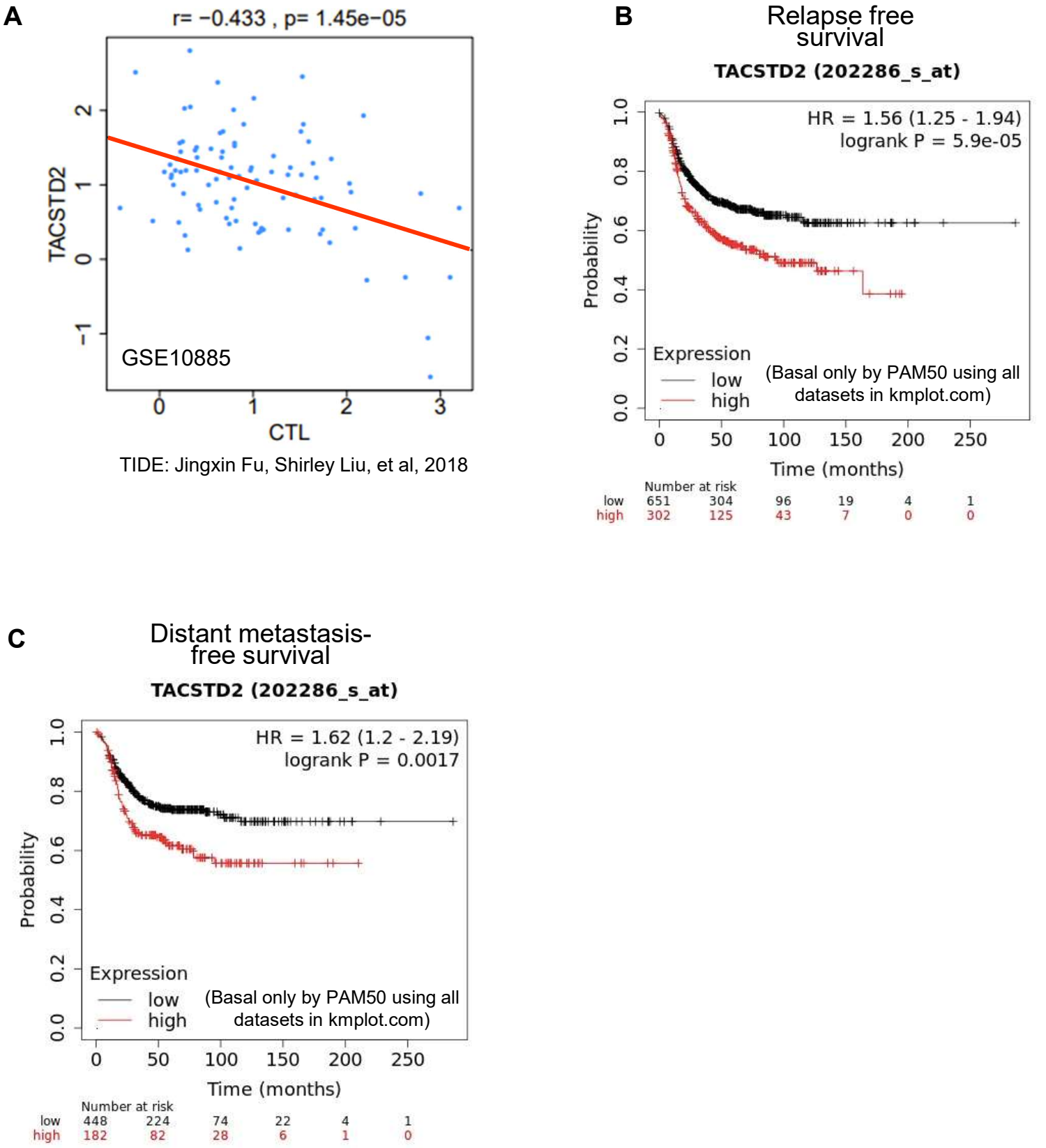

Supplemental Figure S2. TROP2 promotes AT-3 mammary tumor growth and immune exclusion in immunocompetent hosts

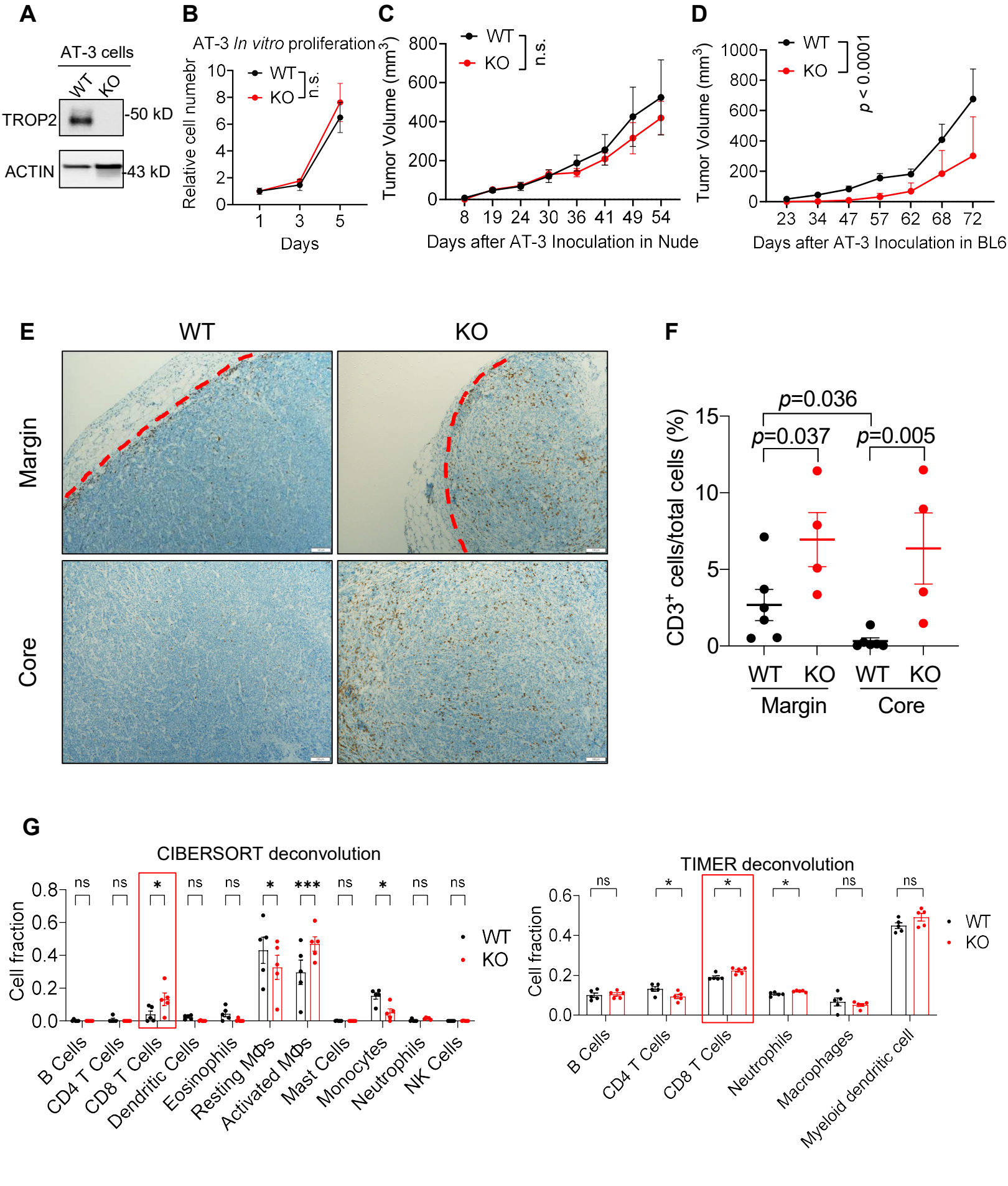

Supplemental Figure S3. RNA-seq analysis for WT and KO 4T1 tumors and TROP2 reconstitution

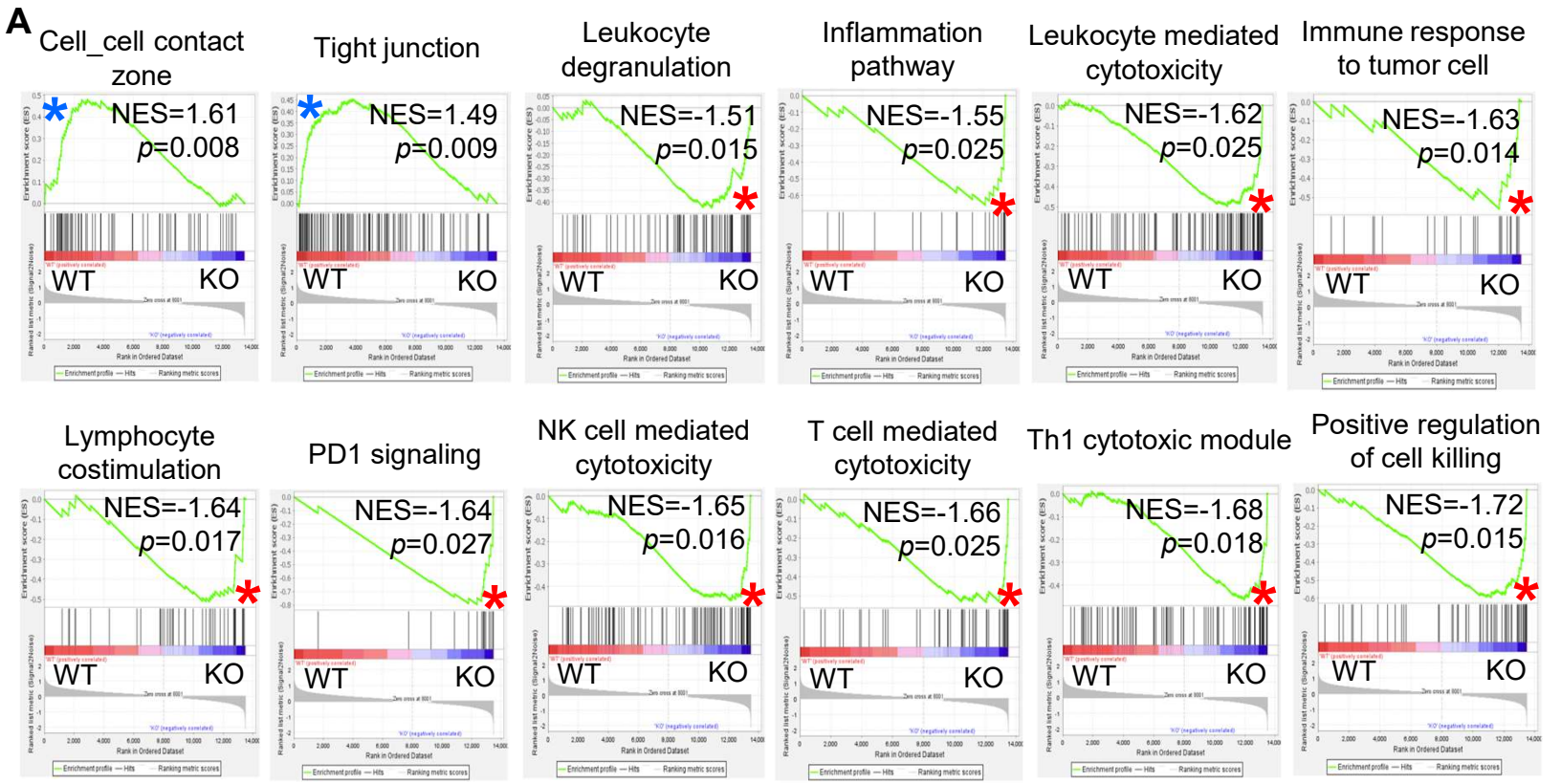

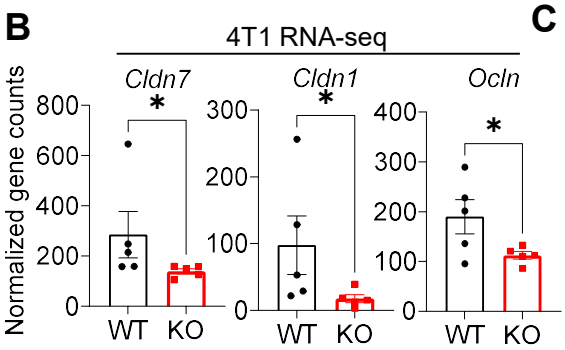

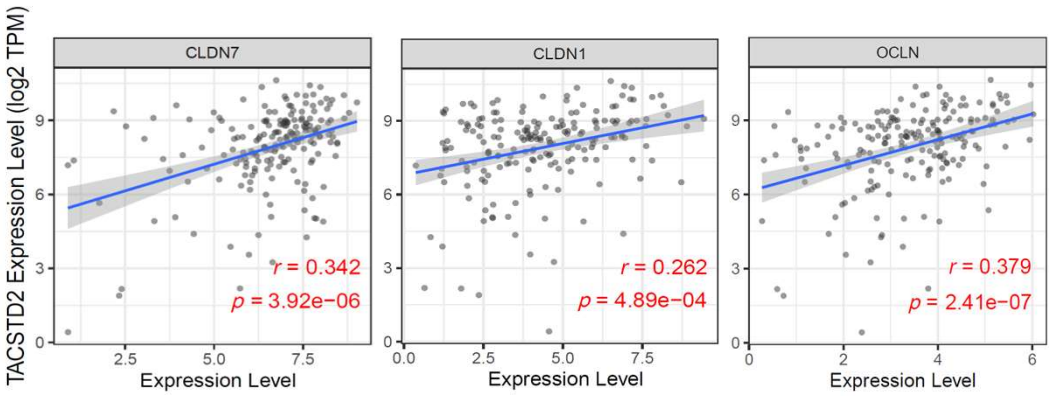

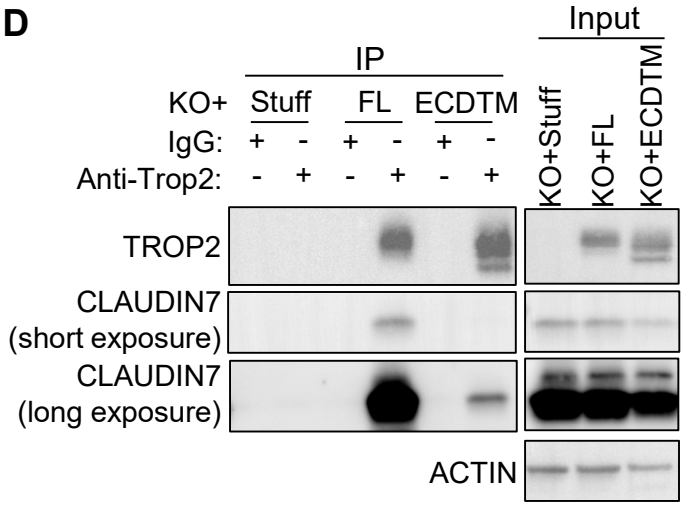

Supplemental Figure S4: human TROP2 reconstitution in 4T1 *Trop2*-KO tumor

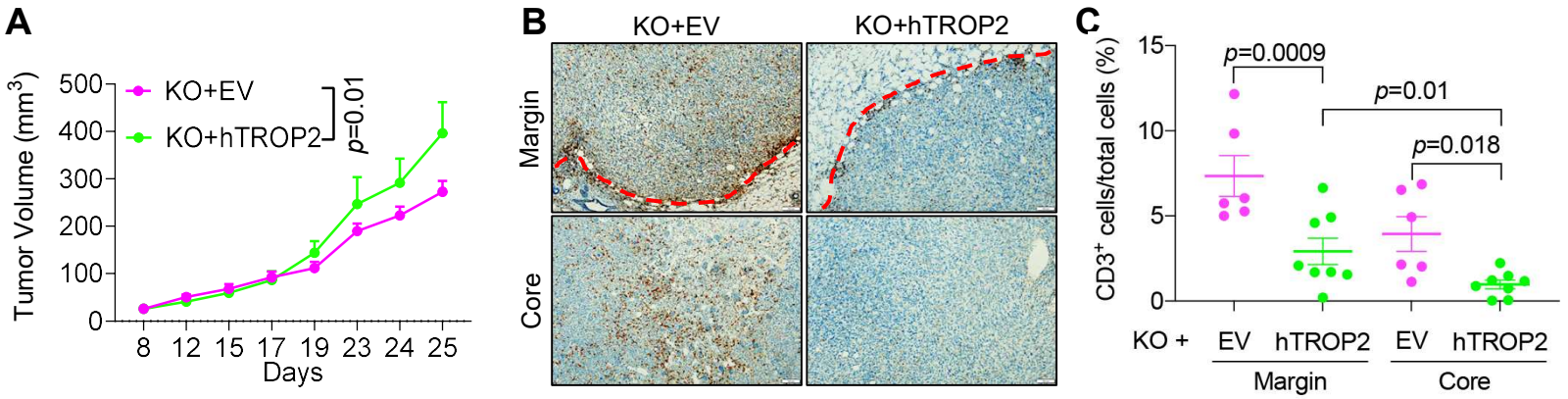

Supplemental Figure S5. Correlations between TACSTD2 and immune checkpoint inhibitor response